

# DNFOMP: Dynamic Neural Field Optimal Motion Planner for Navigation of Autonomous Robots in Cluttered Environment

Maksim Katerishich, Mikhail Kurenkov, Sausar Karaf, Artem Nenashev, and Dzmitry Tsetserukou

**Abstract**—Motion planning in dynamically changing environments is one of the most complex challenges in autonomous driving. Safety is a crucial requirement, along with driving comfort and speed limits. While classical sampling-based, lattice-based, and optimization-based planning methods can generate smooth and short paths, they often do not consider the dynamics of the environment. Some techniques do consider it, but they rely on updating the environment on-the-go rather than explicitly accounting for the dynamics, which is not suitable for self-driving. To address this, we propose a novel method based on the Neural Field Optimal Motion Planner (NFOMP), which outperforms state-of-the-art approaches in terms of normalized curvature and the number of cusps. Our approach embeds previously known moving obstacles into the neural field collision model to account for the dynamics of the environment. We also introduce time profiling of the trajectory and non-linear velocity constraints by adding Lagrange multipliers to the trajectory loss function. We applied our method to solve the optimal motion planning problem in an urban environment using the BeamNG.tech driving simulator. An autonomous car drove the generated trajectories in three city scenarios while sharing the road with the obstacle vehicle. Our evaluation shows that the maximum acceleration the passenger can experience instantly is  $-7.5 \text{ m/s}^2$  and that 89.6% of the driving time is devoted to normal driving with accelerations below  $3.5 \text{ m/s}^2$ . The driving style is characterized by 46.0% and 31.4% of the driving time being devoted to the light rail transit style and the moderate driving style, respectively.

## I. INTRODUCTION

Autonomous robotics is experiencing rapid growth, with major companies announcing plans to sell driving automation technologies. However, ensuring automotive safety remains a key challenge for the development and commercialization of autonomous vehicles. Motion planning is crucial for self-driving cars to generate a safe and efficient path, but it is challenging due to the car’s complex shape, non-holonomic constraints, and changing environments [1].

The recently presented NFOMP: Neural Field Optimal Motion Planner [2] successfully overcomes most of the problems of sample-based, lattice-based, and optimization-based planners. It is significantly superior to the most state-of-the-art approaches, outperforming them by 25% on normalized curvature and by 75% on the number of cusps, but it was presented only in a static environment. To improve the NFOMP, we modified the trajectory optimizer to generate a time-profiled trajectory and incorporated known obstacle dynamics into the neural field collision model. A visualization of the planner is shown in Fig. 1. We demonstrate that the

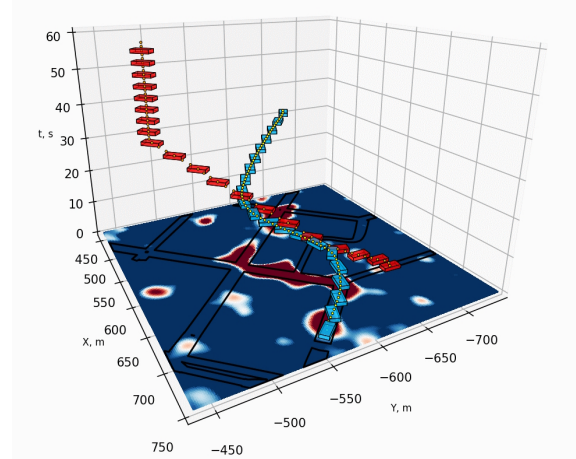


Fig. 1: DNFOMP graphical representation. Dark red is the low obstacle neural field value. Dark blue is the high obstacle neural field value. Blue and red bounding boxes represent sequential positions of the Ego vehicle and obstacle vehicle in time. Black lines are road edges.

resulting trajectory has sufficient driving comfort parameters and has no collisions by launching an autonomous car to ride along several trajectories in the presence of other vehicles on the road in the BeamNG.tech simulator [3]. We collected data from the simulator’s on-board accelerometer and showed that accelerations that affect a “virtual passenger” are admissible.

**Thus, the main contributions of this work are:**

- a neural field representation of collisions, that accounts for the moving obstacles;
- a trajectory optimization method for a self-driving car with velocity and steering constraints;
- an optimization-based algorithm for optimal motion planning of planar non-circular non-holonomic robots.

## II. RELATED WORK

An exact combinatorial solution for motion planning is impossible as it is proven to be PSPACE-hard [4]. The only way to solve the motion planning problem is to find inexact solutions. The prior work in this area can be classified according to the approach used to find an initial path or optimize the prior trajectory.

There are existing random sampling-based approaches to the problem of highway planning based on sampling in spatio-temporal space, such as ST-RRT\* [5] and SCATE [6]. These planners can quickly achieve a feasible path; however, they do not provide smooth and short trajectories, and further processing of such a trajectory is required [7]. Moreover,

The authors are with the Intelligent Space Robotics Laboratory, Skoltech, Bolshoy Boulevard 30, bld. 1, 121205, Moscow, Russia  
 Email: {Maksim.Katerishich, Mikhail.Kurenkov, Sausar.Karaf, Artem.Nenashev, D.Tsetserukou}@skoltech.ru

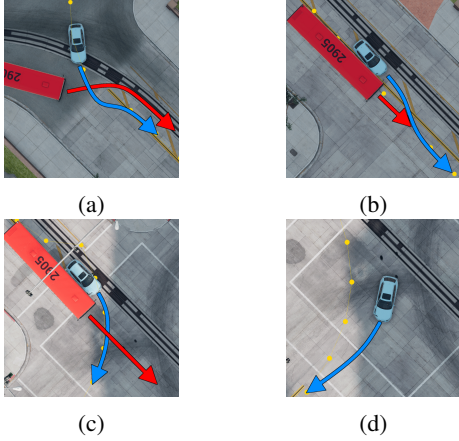


Fig. 2: Limitations of the continuous replanning methodology. The blue vehicle is the Ego vehicle, the red vehicle is the Obstacle vehicle, and the yellow line shows the planned trajectory. The blue and Red arrows show the direction of driving of the Ego and Obstacle vehicles, respectively.

adding more dimensions to the planning space generates an additional problem of computational complexity that should be conditioned and solved in special ways [8].

Another approach to this is to have a set of spline trajectories [9] or to build the trajectory using a conformal spatio-temporal lattice [8]. The benefit of this approach is that it ultimately produces smooth and plain trajectories, as they are essentially parametrized curves. However, such trajectories represent a predefined set, and the universal applicability of the approach is the main drawback [10].

Using neural networks is considered for the motion planning problem. The efficiency of such approaches is reached by combining them with other algorithms and using these networks as advisors for constrained problems, such as the selection of spline anchor points [11] or recommending a local goal for an MPC [12]. The main drawback of such an approach is still the requirement of supervised learning, which raises the question of validation under varying conditions. As one of the most outstanding examples, an optimization-based planner was used back in 2005 in Alice for the DARPA Grand Challenge [13]. The commonly used approaches rely on artificial potential fields or precomputed signed distance functions [14], which are then improved by various algorithms to overcome known shortcomings. Also, they do not often account for dynamic obstacles [15].

### III. METHODOLOGY

This section describes the proposed dynamic neural field optimal motion planner (DNFOMP). First, we describe the limitations of the continuous replanning methodology. Subsequently, we cover the proposed novel dynamic obstacle neural field model. Then, we discuss the added Lagrange multipliers and loss functions for trajectory optimization.

#### A. Continuous replanning

At first sight, the problem of a dynamic environment can be solved in a simpler way. If the positions of obstacles

are updated in each planning step, then the movement of obstacles can be considered. Collision model loss is then an output of the continuously updated neural field with the BCE logit loss function as follows:

$$L_{onf} = \frac{1}{N} \sum_{i=0}^N (BCElogit(F_{\Theta}^j(x_i, y_i, \theta_i), o_i), j = 0, 1, 2, \dots, M) \quad (1)$$

Here, we represent the SE (2) trajectory positions with  $x$  and  $y$  coordinates in the absolute frame, and  $\theta$  heading angle;  $F_{\Theta}^j(x_i, y_i, \theta_i)$  is the neural network parametrized with  $\Theta$  parameters,  $N$  is the number of positions in the trajectory,  $M$  is the horizon of the planning task, and  $o_i$  is the ground truth collision measured by the collision function.

Such a straightforward approach does not perform well in a basic driving scenario. As shown in Fig. 2, the blue Ego vehicle is driving down the street and ready to turn right. The red obstacle vehicle drives in the same direction at the same speed. The relative positions of the vehicles are constant, and the planned trajectory can always be found ahead of the vehicles. The Ego vehicle is not able to turn unless the obstacle is far enough away and the optimizer is able to build another path. In certain cases, this can lead to aggressive braking, extensive steering, or a collision.

#### B. Dynamic Neural Field Obstacle Model

We enable the collision model to consider not only the instant picture of the environment at a time step, but also the time-spanned collisions by extending the planning space. We introduce a new state variable,  $t$ , which stands for time. This makes all obstacles time-dependent. In this work, we set the trajectories of the obstacles based on prior knowledge. The adaptive nature of the neural field allows it to handle uncertainties; hence, the ground truth of the trajectory can be replaced with the estimation of one without any modification of the method but with hyperparameter tuning. We assume such prior knowledge of the obstacle trajectory to be sufficient for the method's validation. Thus, collision model loss is an output of the dynamic neural field with the BCE logit loss function as follows:

$$L_{dnf} = \frac{1}{N} \sum_{i=0}^N (BCElogit(F_{\Theta}(x_i, y_i, \theta_i, t_i), o_i) \quad (2)$$

Here, we represent trajectory positions with  $x$ ,  $y$  coordinates in the absolute frame,  $\theta$  heading angle, and time  $t$ , which means that we may or may not have a collision at the same SE(2) point in the planning space, depending on the time when collision is checked. This neural network consists of three hidden layers with 128 neurons, each with a ReLU activation function.

Thus, we introduce the ambiguity of the planning space. The trajectory optimizer can choose either to change the path itself in the spatial domain or modify the velocity profile to make the car brake or accelerate.

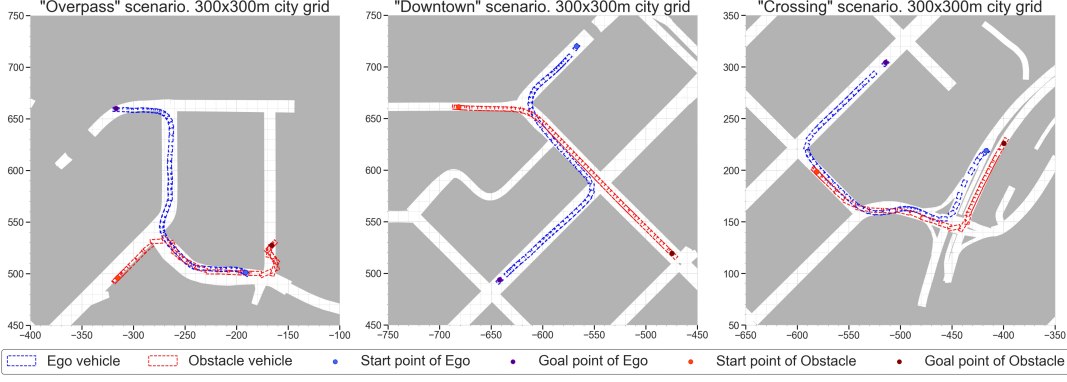


Fig. 3: Trajectories generated by DNFOMP in the test scenarios. Blue and red bounding boxes represent the sequential positions of the Ego and the obstacle vehicles, respectively. Gray and white are restricted and drivable zones, respectively.

TABLE I: Numerical values of loss function weights

Term	Value
Distance loss weight	$5 \cdot 10^1$
Collision loss weight	$5 \cdot 10^4$
Non-holonomic constraints loss weight	$5 \cdot 10^1$
Maximum velocity loss weight	$1 \cdot 10^2$
Time regularization loss weight	$1 \cdot 10^2$

### C. Trajectory optimization in a dynamic environment

Planning space is no longer planar but volumetric, where the third axis is time. To handle this ambiguity and consider that collision can be avoided in the spatial domain or in the temporal domain, we propose to add two more terms for trajectory loss building in addition to the original paper's trajectory loss terms. The first term is the velocity constraint. The goal of this constraint is to maintain the desired speed while driving. We use Lagrange multipliers that are multiplied by constraint deltas that should be zero and maximized during optimization. We used velocity constraint deltas  $\delta_i$  from the equation:

$$\delta_i = v_e(t_{i+1} - t_i) - \sqrt{(x_{i+1} - x_i)^2 + (y_{i+1} - y_i)^2 + (\theta_{i+1} - \theta_i)^2} \quad (3)$$

Here,  $v_e$  is the desired velocity of the Ego vehicle. Thus, the velocity constraint loss  $L_{vel}$  is given as follows:

$$L_{vel} = \frac{1}{N} \sum_{i=0}^N (\delta_i^2 - \lambda_i \delta_i) \quad (4)$$

where  $\lambda_i$  are the Lagrange multipliers.

The second term is the time regularization loss. The goal of this term is to penalize the uneven spacing of time intervals in the trajectory. This is aimed at minimizing longitudinal acceleration during driving. The time regularization loss  $L_{time}$  is given as follows:

$$L_{time} = \frac{1}{N} \sum_{i=0}^N (t_{i+1} - t_i)^2 \quad (5)$$

Additionally, we include a modified trajectory reparametrization algorithm. In the original work,

reparametrization is about generating a set of interpolated positions between successive trajectory points, to achieve a uniform spacing of positions. We first need to align time intervals and then sample interpolated positions. The newly distributed time values  $t_i^{new}$  are:

$$t_i^{new} = i \frac{t_N}{N-1}, \quad i = 0, 1, 2, \dots, N \quad (6)$$

Then, we calculate the collision loss for trajectory optimization as follows:

$$L_{col} = \frac{1}{N-1} \sum_{i=0}^{N-1} (\text{softplus}(F_{\Theta}(\tilde{x}_i, \tilde{y}_i, \tilde{\theta}_i, t_i^{new}))) \quad (7)$$

where  $(\tilde{x}_i, \tilde{y}_i, \tilde{\theta}_i)$  is the interpolated position randomly chosen between  $(x_i, y_i, \theta_i)$  and  $(x_{i+1}, y_{i+1}, \theta_{i+1})$ .

### D. Final Loss for Trajectory Optimization

Thus, the final loss function consists of four parts: the collision loss function  $L_{col}$ , which pushes a trajectory away from collisions; the original paper trajectory loss terms, which are non-holonomic constraints  $L_{constr}$  that force the trajectory to be smooth and Laplacian regularization  $L_{dist}$  that shortens the overall path; velocity constraints  $L_{vel}$  that force the vehicle to maintain constant speed along the trajectory; and time regularization  $L_{time}$  that forces the velocity profile to be as plain as possible. The constraint loss, as well as the maximum velocity loss, includes two terms: quadratic and linear with Lagrange multipliers. For collision loss, we use the softplus function on the output of the neural network. Thus, the resulting trajectory loss can be calculated from:

$$L_{traj} = w_{dist} L_{dist} + w_{col} L_{col} + w_{constr} L_{constr} + w_{vel} L_{vel} + w_{time} L_{time} \quad (8)$$

where  $w$  is the weight that corresponds to each of the terms. The numerical values are provided in Table I. In the following section, we conducted a sensitivity analysis of how the weight ratio affects the trajectory.



### E. Details of optimization

The optimization is based on the Adam optimizer [16] for both the obstacle neural field model and the trajectory loss. For the neural field obstacle model, we use learning rate of  $1 \cdot 10^{-1}$  and betas of (0.9,0.9). In contrast to the original work, we use cyclic learning rate scheduling for trajectory optimization, which switches the learning rate between  $1 \cdot 10^{-2}$  and  $1 \cdot 10^{-1}$ , with betas of (0.9,0.9). This helps to traverse the local minima faster and reduce the planning time. Learning rates are correlated to each other for stable planning. The Lagrange’s multipliers are optimized with the learning rate of  $1 \cdot 10^{-1}$ .

Gradients of the loss function are preconditioned based on an inverse of pseudo Hessian, as in the article [17], that is the sum of the quadratic form matrix and the identity matrix with coefficients. For gradient preconditioning, we use the following equation:

$$g_i = \begin{bmatrix} \eta(\alpha H + I)^{-1} \nabla(L_{traj}^P) \\ \eta(\alpha H + I)^{-1} \nabla(L_{traj}^T) \end{bmatrix} \quad (9)$$

Here  $\eta$  is the learning rate;  $\alpha$  is the hyperparameter that equals 5;  $H$  is the Hessians of  $L_{traj}^*$ , where  $*$  stands for two different components: a  $P$  part that carries the spatial path of the trajectory, i.e., all SE(2) points of it; and the second part  $T$  that carries the temporal part of the trajectory, i.e., time values. The fact that we precondition these gradients separately without making a higher-dimensional Hessian allows us to tune trajectory loss function weights independently. Thus,  $\eta(\alpha H + I)^{-1}$  is calculated once at the beginning of optimization, as Hessian is independent of an optimized trajectory.

For the validation of our method, the PyTorch framework is used for automatic differentiation. The developed code is available online at GitLab<sup>1</sup>.

## IV. EXPERIMENTS AND RESULTS

### A. Implementation Details

To evaluate the performance of the proposed DNFOMP planner, we used the BeamNG.tech car simulator. It is a scenario-based testing environment for self-driving applications that thoroughly simulates the physics of driving. It has an "AI Vehicle" agent that controls a vehicle and follows the given trajectory. We launched this agent to ride along several trajectories in the presence of other vehicle.

The path-following algorithm of the agent is inaccessible due to its implementation in BeamNG.tech. Besides, the agent is unaware of the full trajectory. It follows the trajectory on a short horizon, a few positions ahead of the current one. It is essential for the trajectory to be uniformly parameterized both in the spatial and temporal domains, in order to let the agent traverse it. In fact, trajectory and agent are not coupled at all. It fails and causes collisions due to a high discrepancy between planned and executed positions

TABLE II: Planning statistics for the test scenarios

Planner	Time, s	Path length, m	Cusps	Max curv.	Norm curv.	AOL · 10 <sup>-3</sup>
<b>Scenario: Downtown</b>						
NFOMP	32.6	321.7	1	0.12	10.9	1.05
DNFOMP	38.1	302.5	0	0.05	8.15	0.85
<b>Scenario: Crossing</b>						
NFOMP	34.2	360.1	0	0.07	12.6	1.0
DNFOMP	41.9	344.7	0	0.07	10.2	0.9
<b>Scenario: Overpass</b>						
NFOMP	28.8	281.2	0	0.21	17.0	1.1
DNFOMP	36.8	264.9	0	0.10	13.4	2.1

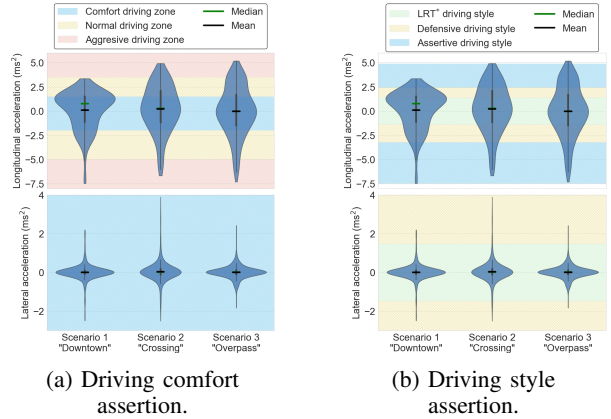


Fig. 4: Lateral and longitudinal accelerations of the Ego vehicle while driving the planned trajectories.

\* Light Rail Transport.

if bad trajectory parameters are provided. Thus, this makes this agent a reasonable validation tool.

The following metrics were obtained: The first group depicts properties of the path: computation time in seconds (s); path length in meters (m); cusps are the number of abrupt changes of robot direction; the maximum and normalized curvature (lower is better); and angle-over-length (AOL) is the smoothness of the generated path. The second group shows the properties of driving along the trajectory. They are the longitudinal and lateral accelerations, which are obtained via the simulated accelerometer placed on the driver’s headrest, and the trajectory following error, which is the Euclidean distance between actual and planned positions in time.

Experiments were conducted in the presence of a single moving obstacle vehicle. In each scene, five experiments with the same start and goal points were launched. The test cases included three different scenarios, which are 300x300 m city grids; see Fig. 3. In each of them, a single moving obstacle is launched. A trajectory was initialized with the A\* algorithm. The video of the simulation is available on YouTube<sup>2</sup>.

### B. Path Properties Evaluation

We compared the proposed DNFOMP and the original NFOMP in light of the metrics of the first group. For the NFOMP, we did not take any moving obstacles into account. Also, we did not include metrics of the second group, as they do not correspond to the same driving modes: without the

<sup>1</sup><https://gitlab.com/kukaruka/pytorch-motion-planner>

<sup>2</sup><https://youtu.be/yae14JM2-OI>

TABLE III: Relation between control stiffness of the agent and vehicle settings

Control stiffness	Brake force multiplier	Throttle strength multiplier
1.0	1.0	1.0
0.7	0.7	0.22
0.5	0.5	0.12
0.2	0.2	0.08
0.1	0.1	0.05

presence of obstacles, the optimal spacing of the values is linear, while the presence of obstacles requires deforming the trajectory and using braking and acceleration. The results are presented in Table II. The proposed planner is able to keep similar trajectory metrics together with moving obstacle collision avoidance. Moreover, the method is dimension-agnostic, as the increased number of dimensions of the planning space did not affect planning time significantly.

### C. Dynamic Properties Evaluation

This section presents the results of the experiments in light of the metrics of the second group. The desired speed is set to 40 kph. The Ego vehicle car model is set to “ETK-800”, which corresponds to a mid-range wagon that is capable of producing up to 1G overload ( $9.81 \text{ m/s}^2$  acceleration magnitude) during driving with this setup. Full braking was allowed, and default throttle strength was enabled for the vehicle. For the evaluation, we used assigned zones with respect to accelerations.

The comfort, normal, and aggressive ranking of driving an autonomous shuttle bus is proposed in [18]. The authors opted for a driving style that would be accepted by a cautious passenger. According to this study, the interquartile range of longitudinal acceleration is within the normal driving zone in all test scenarios. The maximum acceleration reaches  $5.0 \text{ m/s}^2$ , and the maximum deceleration (braking) reaches  $-7.5 \text{ m/s}^2$ , which are within acceptable zones. Based on longitudinal acceleration, on average 54.9%, 34.7%, and 10.3% of driving time are devoted to comfort, normal, and aggressive driving, respectively. The evaluation is presented in Fig. 4a.

Another categorization is proposed in [19]. The authors assess the driving style of autonomous vehicles based on the feedback of human drivers who were passengers in the vehicle. Participants agreed with the defensive (moderate) style and found the light rail transit driving style too tedious and the assertive style too rough. Based on longitudinal acceleration, the driving style of the agent corresponds to the light rail transport style at 46.0% of driving time, to the defensive and assertive styles at 31.4% and 26.6% of driving time, respectively. The evaluation is presented in Fig. 4b.

We validated the quality of trajectory parametrization by introducing the “control stiffness” parameter, which is an aggregate of explicitly limiting brake force and implicitly reducing throttle strength of the vehicle, as shown in Table III. With 1.0 control stiffness, the maximum trajectory following error is 0.67 m and the maximum longitudinal acceleration is  $4.5 \text{ m/s}^2$ . While reducing the stiffness down to 0.5, the acceleration remains above  $4 \text{ m/s}^2$  and the error is slightly increased. With the significant reduction in control stiffness

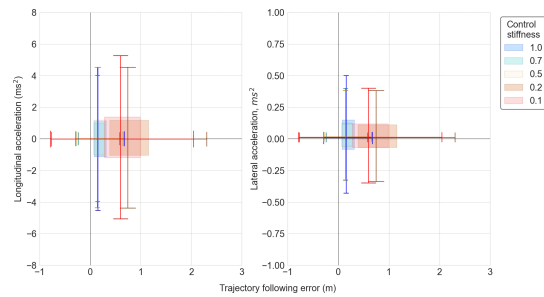


Fig. 5: Trajectory following error and corresponding accelerations of the Ego vehicle depending on control stiffness.

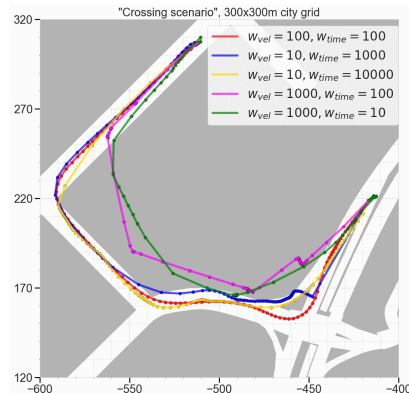


Fig. 6: Sensitivity analysis of different parameters.

down to 0.2, the error increases rapidly to 2.5 m. Therefore, the trajectory is parametrized in such a way that the agent executes it with the desired parameters while having the capability to drive more aggressively. Unless this capability is below the requirements of the planning algorithm, it succeeds in providing considerable route following, as shown in Fig. 5.

### D. Sensitivity analysis

We conducted a sensitivity analysis to show the influence of time regularization weight and velocity constraint weight on trajectory quality. Fig. 6 shows that the ratio of these weights should be close to 1. If the time regularization weight dominates the velocity constraint weight, the trajectory becomes ill-parametrized in the space domain. The result is point clustering around high collision zones, where the velocity is lower than in the rest of the trajectory. If the velocity constraint weight dominates the time regularization weight, the trajectory becomes ill-parametrized in the time domain, and shortcutting can appear. The result is trajectory shrinking and point clustering around zones where time values are close.

## V. CONCLUSION AND FUTURE WORK

We have presented a novel algorithm to solve the optimal motion planning problem for a self-driving car in cluttered urban environments. This algorithm, due to embedding environment dynamics into the neural field collision model, makes it possible to plan a trajectory in spatio-temporal space and avoid moving obstacles. To validate the

proposed method, an autonomous vehicle drove along the planned trajectories in the BeamNG.tech driving simulator. Conventional metrics such as trajectory curvature and the number of cusps were obtained. In these terms, the proposed approach is at the same level as the NFOMP baseline, and moving obstacles are considered additionally. According to the study of dynamic properties, the maximum acceleration that a passenger can experience instantly is  $-7.5 \text{ m/s}^2$ , and 89.6% of the driving time is devoted to normal driving with accelerations below  $3.5 \text{ m/s}^2$ ; the assertion of driving style shows that 46.0% and 31.4% of the driving time are devoted to the light rail transit style and the moderate driving style, respectively.

In the future, we plan real-world experiments on various setups, for example, outdoor [20]–[22] and indoor [23]–[26] mobile robots, UAVs [27]–[31], as well as examine the applicability of the approach to more sophisticated systems, e.g., modular two-wheeled rovers [32].

## REFERENCES

- [1] J. Wang, L. Zhang, Y. Huang, and J. Zhao, “Safety of autonomous vehicles,” *Journal of Advanced Transportation*, vol. 2020, p. 8867757, Oct 2020.
- [2] M. Kurenkov *et al.*, “Nfomp: Neural field for optimal motion planner of differential drive robots with nonholonomic constraints,” *IEEE Robotics and Automation Letters*, vol. 7, no. 4, pp. 10991–10998, 2022.
- [3] M. Pascale *et al.*, “Beamng.tech technical paper,” *BeamNG GMBH*, 2021.
- [4] S. M. LaValle, *Planning Algorithms*. Cambridge University Press, 2006.
- [5] F. Grothe, V. N. Hartmann, A. Orthey, and M. Toussaint, “St-rrt\*: Asymptotically-optimal bidirectional motion planning through space-time,” in *2022 International Conference on Robotics and Automation (ICRA)*, pp. 3314–3320, 2022.
- [6] M. King-Smith, P. Tsiotras, and F. Dellaert, “Simultaneous control and trajectory estimation for collision avoidance of autonomous robotic spacecraft systems,” in *2022 International Conference on Robotics and Automation (ICRA)*, pp. 257–264, 2022.
- [7] J. Wang, M. Q.-H. Meng, and O. Khatib, “Eb-rrt: Optimal motion planning for mobile robots,” *IEEE Transactions on Automation Science and Engineering*, vol. 17, no. 4, pp. 2063–2073, 2020.
- [8] M. McNaughton, C. Urmson, J. M. Dolan, and J.-W. Lee, “Motion planning for autonomous driving with a conformal spatiotemporal lattice,” in *2011 IEEE International Conference on Robotics and Automation*, pp. 4889–4895, 2011.
- [9] J. P. Talamino and A. Sanfeliu, “Anticipatory kinodynamic motion planner for computing the best path and velocity trajectory in autonomous driving,” *Robotics and Autonomous Systems*, vol. 114, pp. 93–105, 2019.
- [10] C. Katrakazas, M. Quddus, W.-H. Chen, and L. Deka, “Real-time motion planning methods for autonomous on-road driving: State-of-the-art and future research directions,” *Transportation Research Part C: Emerging Technologies*, vol. 60, pp. 416–442, 2015.
- [11] P. Kicki and P. Skrzypczyński, “Speeding up deep neural network-based planning of local car maneuvers via efficient b-spline path construction,” in *2022 International Conference on Robotics and Automation (ICRA)*, pp. 4422–4428, 2022.
- [12] B. Brito, M. Everett, J. P. How, and J. Alonso-Mora, “Where to go next: Learning a subgoal recommendation policy for navigation in dynamic environments,” *IEEE Robotics and Automation Letters*, vol. 6, no. 3, pp. 4616–4623, 2021.
- [13] L. B. Cremean *et al.*, *Alice: An Information-Rich Autonomous Vehicle for High-Speed Desert Navigation*, pp. 437–482. Berlin, Heidelberg: Springer Berlin Heidelberg, 2007.
- [14] P. Zips, M. Böck, and A. Kugi, “Optimisation based path planning for car parking in narrow environments,” *Robotics and Autonomous Systems*, vol. 79, pp. 1–11, 2016.
- [15] P. F. Lima, *Optimization-Based Motion Planning and Model Predictive Control for Autonomous Driving With Experimental Evaluation on a Heavy-Duty Construction Truck*. PhD dissertation, KTH Royal Institute of Technology, Stockholm, Sweden, 2018.
- [16] D. P. Kingma and J. Ba, “Adam: A method for stochastic optimization,” 2017.
- [17] B. Nicolet, A. Jacobson, and W. Jakob, “Large steps in inverse rendering of geometry,” *ACM Transactions on Graphics*, vol. 40, pp. 1–13, 12 2021.
- [18] I. Bae, J. Moon, and J. Seo, “Toward a comfortable driving experience for a self-driving shuttle bus,” *Electronics*, vol. 8, no. 9, 2019.
- [19] N. Md Yusof, J. Karjanto, J. Terken, F. Delbressine, M. Hassan, and M. Rauterberg, “The exploration of autonomous vehicle driving styles: Preferred longitudinal, lateral, and vertical accelerations,” pp. 245–252, 10 2016.
- [20] S. Protasov, P. Karpyshev, I. Kalinov, P. Kopanov, N. Mikhailovskiy, A. Sedunin, and D. Tsetserukou, “Cnn-based omnidirectional object detection for hermesbot autonomous delivery robot with preliminary frame classification,” in *2021 20th International Conference on Advanced Robotics (ICAR)*, pp. 517–522, IEEE, 2021.
- [21] P. Karpyshev, V. Ilin, I. Kalinov, A. Petrovsky, and D. Tsetserukou, “Autonomous mobile robot for apple plant disease detection based on cnn and multi-spectral vision system,” in *2021 IEEE/SICE international symposium on system integration (SII)*, pp. 157–162, IEEE, 2021.
- [22] P. Karpyshev, E. Kruzhkov, E. Yudin, A. Savinykh, A. Potapov, M. Kurenkov, A. Kolomeitsev, I. Kalinov, and D. Tsetserukou, “Mucaslarm: Cnn-based frame quality assessment for mobile robot with omnidirectional visual slam,” in *2022 IEEE 18th International Conference on Automation Science and Engineering (CASE)*, pp. 368–373, IEEE, 2022.
- [23] N. Mikhailovskiy, A. Sedunin, S. Perminov, I. Kalinov, and D. Tsetserukou, “Ultrabot: Autonomous mobile robot for indoor uv-c disinfection with non-trivial shape of disinfection zone,” in *2021 26th IEEE International Conference on Emerging Technologies and Factory Automation (ETFA)*, pp. 1–7, IEEE, 2021.
- [24] S. Perminov, N. Mikhailovskiy, A. Sedunin, I. Okunevich, I. Kalinov, M. Kurenkov, and D. Tsetserukou, “Ultrabot: Autonomous mobile robot for indoor uv-c disinfection,” in *2021 IEEE 17th International Conference on Automation Science and Engineering (CASE)*, pp. 2147–2152, IEEE, 2021.
- [25] A. Petrovsky, I. Kalinov, P. Karpyshev, M. Kurenkov, V. Ramzhaev, V. Ilin, and D. Tsetserukou, “Customer behavior analytics using an autonomous robotics-based system,” in *2020 16th International Conference on Control, Automation, Robotics and Vision (ICARCV)*, pp. 327–332, IEEE, 2020.
- [26] I. Okunevich, D. Trinitatova, P. Kopanov, and D. Tsetserukou, “Deltacharger: Charging robot with inverted delta mechanism and cnn-driven high fidelity tactile perception for precise 3d positioning,” *IEEE Robotics and Automation Letters*, vol. 6, no. 4, pp. 7604–7610, 2021.
- [27] I. Kalinov, A. Petrovsky, R. Agishev, P. Karpyshev, and D. Tsetserukou, “Impedance-based control for soft uav landing on a ground robot in heterogeneous robotic system,” in *2021 International Conference on Unmanned Aircraft Systems (ICUAS)*, pp. 1653–1658, IEEE, 2021.
- [28] I. Kalinov, E. Safronov, R. Agishev, M. Kurenkov, and D. Tsetserukou, “High-precision uav localization system for landing on a mobile collaborative robot based on an ir marker pattern recognition,” in *2019 IEEE 89th Vehicular Technology Conference (VTC2019-Spring)*, pp. 1–6, IEEE, 2019.
- [29] I. Kalinov, A. Petrovsky, V. Ilin, E. Pristanskiy, M. Kurenkov, V. Ramzhaev, I. Idrisov, and D. Tsetserukou, “Warevision: Cnn barcode detection-based uav trajectory optimization for autonomous warehouse stocktaking,” *IEEE Robotics and Automation Letters*, vol. 5, no. 4, pp. 6647–6653, 2020.
- [30] I. Kalinov, D. Trinitatova, and D. Tsetserukou, “Warevr: Virtual reality interface for supervision of autonomous robotic system aimed at warehouse stocktaking,” in *2021 IEEE International Conference on Systems, Man, and Cybernetics (smc)*, pp. 2139–2145, IEEE, 2021.
- [31] D. Yatskin and I. Kalinov, “Principles of solving the space monitoring problem by multirotors swarm,” in *2017 14th International Conference on Engineering and Telecommunication (EnT)*, pp. 47–50, IEEE, 2017.
- [32] A. Petrovsky, I. Kalinov, P. Karpyshev, D. Tsetserukou, A. Ivanov, and A. Golkar, “The two-wheeled robotic swarm concept for mars exploration,” *Acta Astronautica*, vol. 194, pp. 1–8, 2022.